InAs quantum wells grown on GaP/Si substrate with Ga(In,As)P metamorphic buffers

HUANG Wei-Guo[1,4], 　GU Yi[1,2,3,4*], 　JIN Yu-Hang[2,3], 　LIU Bo-Wen[2,3], 　GONG Qian[1], 　HUANG Hua[1], 　WANG Shu-Min[5], 　MA Ying-Jie[1,2,3], 　ZHANG Yong-Gang[1,2,3]

（1. Key Laboratory of Terahertz Technology，Shanghai Institute of Microsystem and Information Technology，Chinese Academy of Sciences，Shanghai 200050，China；
2. State Key Laboratory of Transducer Technology，Shanghai Institute of Technical Physics，Chinese Academy of Sciences，Shanghai 200083，China；
3. Key Laboratory of Infrared Imaging Materials and Detectors，Shanghai Institute of Technical Physics，Chinese Academy of Sciences，Shanghai 200083，China；
4. University of Chinese Academy of Science，Beijing 100049，China；
5. Department of Microtechnology and Nanoscience，Chalmers University of Technology，Gothenburg SE−41296，Sweden）

Abstract：InAs/In$_{0.83}$Al$_{0.17}$As quantum wells have been demonstrated on In$_{0.83}$Al$_{0.17}$As metamorphic layers on GaP/Si substrates. The effects of Ga$_x$In$_{1-x}$P and GaAs$_y$P$_{1-y}$ graded buffer layers on the sample performances are investigated. The sample with Ga$_x$In$_{1-x}$P metamorphic buffer layer has narrower width in X-ray diffraction reciprocal space maps，indicating less misfit dislocations in the sample. Mid-infrared photoluminescence signals have been observed for both samples at room temperature，while the sample with Ga$_x$In$_{1-x}$P metamorphic buffer shows stronger photoluminescence intensity at all temperatures. The results indicate the metamorphic buffers with mixed cations show superior effects for the mid-infrared InAs quantum wells on GaP/Si composite substrates.

Key words：quantum wells，GaP/Si，metamorphic buffer，mid-infrared

采用 Ga(In,As)P 异变缓冲层的 GaP/Si 衬底上 InAs 量子阱

黄卫国[1,4]，　顾　溢[1,2,3,4*]，　金宇航[2,3]，　刘博文[2,3]，　龚　谦[1]，　黄　华[1]，　王庶民[5]，
马英杰[1,2,3]，　张永刚[1,2,3]

（1. 中国科学院上海微系统与信息技术研究所 太赫兹技术重点实验室，上海 200050；
2. 中国科学院上海技术物理研究所 传感技术联合国家重点实验室，上海 200083；
3. 中国科学院上海技术物理研究所 红外成像材料与器件重点实验室，上海 200083；
4. 中国科学院大学，北京 100049；
5. 查尔姆斯理工大学 微技术与纳米科学系，哥德堡 SE−41296）

摘要：本工作在 GaP/Si 衬底上基于 In$_{0.83}$Al$_{0.17}$As 异变缓冲层实现了 InAs/In$_{0.83}$Al$_{0.17}$As 量子阱的生长。研究了 Ga$_x$In$_{1-x}$P 和 GaAs$_y$P$_{1-y}$ 递变缓冲层对量子阱结构材料性能的影响。采用 Ga$_x$In$_{1-x}$P 组分渐变缓冲层的样品 X 射线衍射倒易空间衍射峰展宽更小，表明样品中的失配位错更少。两个样品均在室温下实现了中红外波段的光致发光，而采用 Ga$_x$In$_{1-x}$P 组分渐变缓冲层的样品在不同温度下都具有更高的光致发光强度。这些结果表明在 GaP/Si 复合衬底上采用阳离子混合的渐变缓冲层对生长中红外 InAs 量子阱结构具有相对更优的效果。

关　键　词：量子阱；GaP/Si；异变缓冲层；中红外

中图分类号：TN215　　　　　　　　　　　　　　　　　**文献标识码**：A

Introduction

Silicon-based photonics has attracted much attention in the past decade, where silicon is utilized as functional devices or supplies a platform for functional devices. In a silicon-based compact optoelectronic sensor system, silicon works as a platform for various devices, including light source, photodetector, and etc [1-3]. For the gas sensing, many fingerprint spectra are located in the mid-infrared (MIR) wavelength range, which makes MIR light sources great potential in the areas such as trace-gas measurement, medical detection, as well as environmental monitoring [4-6]. MIR light source on silicon substrate becomes one of the necessary parts of a compact optoelectronic sensor. Because the III-V compound semiconductors are direct band gap materials with a relatively high light emission efficiency, a practicable method to realize silicon-based MIR light source is to integrate III-V compound semiconductors on the silicon substrate [7-9]. Meanwhile, quantum-wells (QWs) structures have high restrictions for carrier transport. Hence, direct integration of high efficiency III-V QWs on Si substrates has been employed to obtain silicon-based MIR light sources [10, 11]. For example, Nguyen-Van et al. have reported the InAs/AlSb quantum cascade lasers directly grown on Si substrate with the lasers emitting near 11 μm at RT [12]. The type-I InAs MIR QW lasers have been demonstrated [13, 14]. The integration of the InAs QW laser structures on Si substrates is a promising candidate to realize MIR lasers. Mainly three methods exist to integrate group III-V and Si materials, including hybrid integration, wafer bonding and monolithic heteroepitaxy [15]. Among them, the monolithic heteroepitaxial technology with the integrated growth has been reported widely on near-infrared lasers[16-18]. However, only a few reports related to efficient silicon-based MIR light source by the monolithic heteroepitaxial technology are reported up to now.

Growth of III-V semiconductor laser structures on Si substrates usually encounters several main obstacles [19]. Among them, the misfit dislocations originated from the Si/III-V interface deteriorate the laser performances dramatically. Deserve to be mentioned, III-V semiconductor gallium phosphide (GaP) is nearly lattice-matched to Si with low dislocation density [20]. Besides, influenced by different polarities of the interface between the III-V semiconductor and the underlying Si substrate, the antiphase domain (APD) boundaries could form to induce many defects [21, 22]. Several solutions have been proposed to overcome the APDs. Volz et al. have verified that thin GaP nucleation layer grown on Si buffer layer by a flow rate modulated mode could achieve a charge neutral interface [23]. Thus, GaP could be used as a useful template candidate for the growth of III-V semiconductor on Si. Therefore, the monolithic heteroepitaxy of InAs QW lasers on the GaP/Si composite substrate is a feasible method to realize silicon-based MIR light sources. However, the lattice mismatch between the GaP/Si substrate and the InAs epitaxy layer is remarkable. The misfit dislocations arising from the interface could increase non-radia-

tion recombination and meanwhile increase the threshold current density of the lasers. The introduction of a buffer layer has been proved to be an efficient method to filter the dislocations and improve the crystal quality [24-26]. The high-quality InAs quantum dot layers on Si substrates by using a GaAs buffer have been demonstrated [27]. However, few reports related to Si-based InAs QWs through appropriate buffer layers are reported up to now. In this case, the introduction of metamorphic buffers (MBs) has been implemented to improve quality of the InAs QWs on GaP/Si substrates.

In our previous work, type-I InAs/$In_{0.83}Al_{0.17}As$ QWs have been grown on GaP substrates by using $In_{0.83}Al_{0.17}As$ buffers [28]. The misfit dislocations result in the inferior lattice quality as well as the relatively low PL intensity caused by abundant non-radiative recombination centers. In this work, we proposed different pathways of MBs to relax the interface stress as well as to restrain propagation of the threading dislocations originated from the GaP homoepitaxy and the GaP/Si substrate [29]. The heterogeneous silicon-based InAs/$In_{0.83}Al_{0.17}As$ QW becomes feasible through using compositionally graded Ga(In, As)P MBs. The lattice structure and optical properties as well as strain conditions were analyzed to compare the effect of the MBs on the GaP/Si substrates. Results indicate that the sample with the $Ga_xIn_{1-x}P$ buffer shows stronger PL intensity as well as a lower misfit dislocation density.

1 Experiments

The InAs/$In_{0.83}Al_{0.17}As$ QWs were grown by using a VG Semicon V80H gas source molecular beam epitaxy (GSMBE) system on (001)-oriented GaP/Si substrates. Before growth, the substrates were performed through a thermal oxide desorption process. The surface oxide layers on the GaP/Si substrate were desorbed under the P_2 atmosphere at 740 ℃ (measured by thermal couple), then the homoepitaxial GaP buffer layers were grown.

In this study, the main motivation is to preliminarily evaluate the effects of mixed cation buffer GaInP and mixed anion buffer GaAsP on GaP/Si substrates. The growth temperature and layer thickness of the MBs are important parameters for the material quality. It is known that the appropriate growth temperature of GaAsP layer is higher than GaInP. The appropriate growth temperatures were set for the respective materials based on our experience. To obtain the same strain relaxation, the close grading rates of the MBs are designed. During the growth of GaInP and GaAsP MBs, the lattice constant changes from that of GaP layer to that of InP layer and GaAs layer, respectively. Under the same thickness of the MBs, the sample structure with InGaP has a larger grading rate than the structure with GaAsP in the MBs theoretically. In this case, the layer thickness of the $Ga_xIn_{1-x}P$ metamorphic buffer layer has been designed larger than the $GaAs_yP_{1-y}$ graded buffer layer.

As shown in Fig. 1, sample 1 was grown on GaP/Si substrate and the growth started with a 0.2-μm-thick undoped GaP buffer layer. Then, a 0.2-μm-thick InP layer

was grown on the 0. 9-μm-thick gradient $Ga_xIn_{1-x}P$ buffer layer. After that, a 0. 5- μm-thick $In_zAl_{1-z}As$ MB was grown. The In composition of the $In_zAl_{1-z}As$ layer gradually changed from 0. 52 which is lattice-matched to InP to 0. 83 of the virtual substrate. For sample 2, after undoped GaP buffer layer, the sample structure varies from GaP layer to GaAs layer by growing a 0. 5- μm-thick $GaAs_yP_{1-y}$ MB followed by 0. 2-μm-thick GaAs. Then, a 1-μm-thick $In_zAl_{1-z}As$ MB was grown with the In composition gradually changed from 0 to 0. 83 of the virtual substrate. Similar to the Ga（In，As）P MBs, in order to get the same strain relaxation in the InAlAs MB layers, the InAlAs MB layer in the sample with GaAs has been designed thicker than the other one. Then, a 0. 5-μm-thick $In_{0.83}Al_{0.17}As$ barrier, a 10-nm-thick InAs QW layer and a 10-nm-thick $In_{0.83}Al_{0.17}As$ cap layer were grown for both samples. Besides, the growth temperature of the $Ga_xIn_{1-x}P$ buffer layer was varied from 540ºC to 510 °C with the rate of 0. 007 ºC /s while the effusion cell temperature of Indium and Gallium was continuously increment and decrement, respectively. During the cell operation, the reduction of source flux is prominent after shutter opening. The loss of thermal radiation from the source material surface is responsible for the transient. Therefore, an optimized temperature control is presented to compensate the flux reduction before growth. During the $GaAs_yP_{1-y}$ buffer layer grown, the template temperature was 580 °C. The pressure of AsH_3 and PH_3 was step graded to the corresponding values, respectively. Finally, the growth temperature of the $In_zAl_{1-z}As$ buffer was 510 °C for both samples.

Two different pathways transited from GaP homoepitaxy to $In_{0.83}Al_{0.17}As$ virtual substrate have been depicted by the band-gap versus lattice constant diagram. The transitions of the sample 1 and sample 2 were described by the black line and the red line, respectively. For the sample with $Ga_xIn_{1-x}P$ MBs, the pathway transited from GaP to InP through growing anion gradient $Ga_xIn_{1-x}P$ buffer layer. Then the pathway transited from $In_{0.52}Al_{0.48}As$ which is lattice-matched to InP to $In_{0.83}Al_{0.17}As$ through $In_zAl_{1-z}As$ buffer layer. Similarly, for the sample with $GaAs_yP_{1-y}$ buffer, the anion gradient $GaAs_yP_{1-y}$ buffer layer served as a transition layer for the route changing from GaP to GaAs. The pathway transited from AlAs which is nearly lattice-matched to GaAs to $In_{0.83}Al_{0.17}As$ by using $In_zAl_{1-z}As$ buffer layer ultimately.

2　Results and discussions

After growth, the morphologies of the two samples were observed by adopting a Bruker Dimension-Icon atomic force microscope（AFM）system and shown in Fig. 3. Both samples show regular cross-hatch stripes aligned along the ［110］ and ［1-10］. The root mean square（RMS）roughness values of around 9 nm are similar for both samples.

To evaluate the structural characteristics, the ω-2θ rocking curves as well as the reciprocal space maps（RSMs）were measured using a Philips X'pert MRD high resolution X-ray diffractometer（HRXRD）equipped with a four-crystal Ge（220）monochromator. As shown in Fig. 4, the（004）direction HRXRD ω-2θ scanning curves and the simulated curves of the two samples were described by the black solid and the red dashed line, respectively. For comparing the lattice quality visually, the position of the highest peak of each curve corresponding to Si substrate has been moved to 34. 6º. The relatively broad peaks at about 31. 0º are related to $In_{0.83}Al_{0.17}As$ virtual substrates, because the theoretical peak position
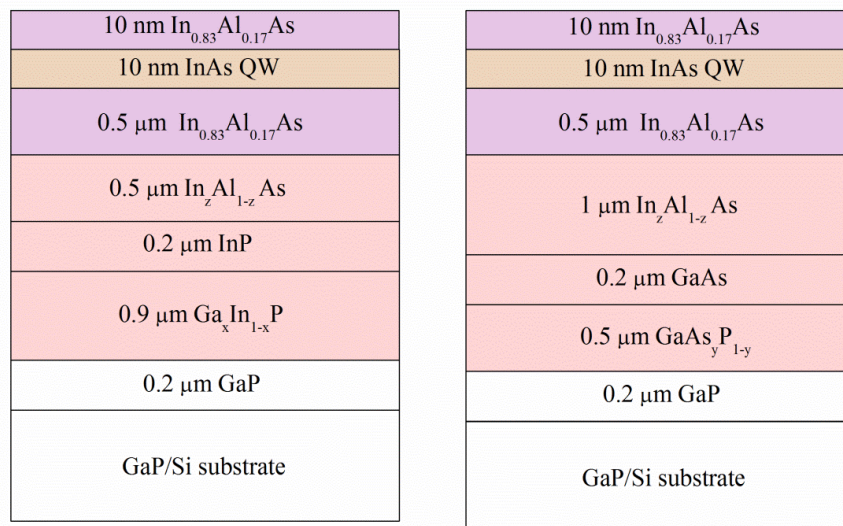
| 10 nm $In_{0.83}Al_{0.17}As$ |
| 10 nm InAs QW |
| 0.5 μm $In_{0.83}Al_{0.17}As$ |
| 0.5 μm $In_zAl_{1-z}As$ |
| 0.2 μm InP |
| 0.9 μm $Ga_xIn_{1-x}P$ |
| 0.2 μm GaP |
| GaP/Si substrate |

| 10 nm $In_{0.83}Al_{0.17}As$ |
| 10 nm InAs QW |
| 0.5 μm $In_{0.83}Al_{0.17}As$ |
| 1 μm $In_zAl_{1-z}As$ |
| 0.2 μm GaAs |
| 0.5 μm $GaAs_yP_{1-y}$ |
| 0.2 μm GaP |
| GaP/Si substrate |

Fig. 1　Schematic structures of the InAs/$In_{0.83}Al_{0.17}As$ quantum wells grown on $Ga_xIn_{1-x}P$ buffer and $GaAs_yP_{1-y}$ buffer
图1　$Ga_xIn_{1-x}P$ 和 $GaAs_yP_{1-y}$ 缓冲层上生长的 InAs/$In_{0.83}Al_{0.17}As$ 量子阱示意图
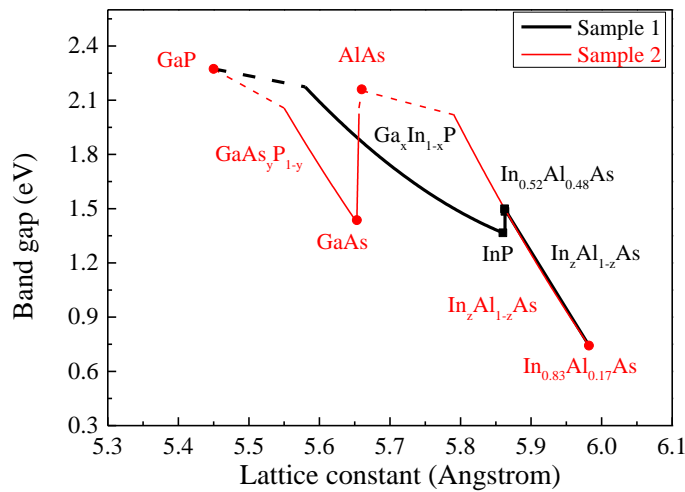
Fig. 2 Lattice constants and band gaps of the InAs/In$_{0.83}$Al$_{0.17}$As quantum wells grown on Ga$_x$In$_{1-x}$P buffer (samples 1) and GaAs$_y$P$_{1-y}$ buffer (samples 2)

图2 Ga$_x$In$_{1-x}$P缓冲层(样品1)和GaAs$_y$P$_{1-y}$缓冲层(样品2)上生长的InAs/In$_{0.83}$Al$_{0.17}$As量子阱结构晶格常数和禁带宽度图

of the In$_{0.83}$Al$_{0.17}$As is at 30.98° in the fully relaxed mode. This indicates that the In$_{0.83}$Al$_{0.17}$As is nearly fully relaxed for both samples. The peaks at about 34.3° are related to the GaP layer, while the weak envelopes around 30.2° appear in the measured curves and are assigned to the peaks of the InAs QW layers according to the simulation. In the simulation of the strain relaxation of InAs QWs, the thicknesses of InAs QWs are less than the critical thicknesses resulting in the planar growth of the InAs layers. Hence, the effects of Ga$_x$In$_{1-x}$P and GaAs$_y$P$_{1-y}$ graded buffer layers on material quality can be investigated adequately through comparing the properties of the InAs QWs. In the simulation, the relaxation degree of InP layer and GaAs layer were nearly fully relaxed for the samples 1 and 2, respectively. The Indium

composition of In$_{0.83}$Al$_{0.17}$As and the InAs QW thickness of 10 nm were used. Besides, the strain relaxation degree of In$_{0.83}$Al$_{0.17}$As layer was set to be 99.3% and 99.1% for samples 1 and 2, respectively. It is obvious that the measured curves match well with the simulated ones. Simultaneously, the simulated values of structural parameters show well consistency with the design ones, indicating that the growth calibrations of alloy mole fraction as well as InAs thickness show good accuracy. Furthermore, it can be observed that the In$_{0.83}$Al$_{0.17}$As peaks of the two samples are nearly the same, with the full widths at half maximum (FWHMs) of 1200 s to the samples. Depend on the results from XRD scanning curves, comparable lattice quality of the samples with Ga$_x$In$_{1-x}$P and GaAs$_y$P$_{1-y}$ buffer could be achieved probably.
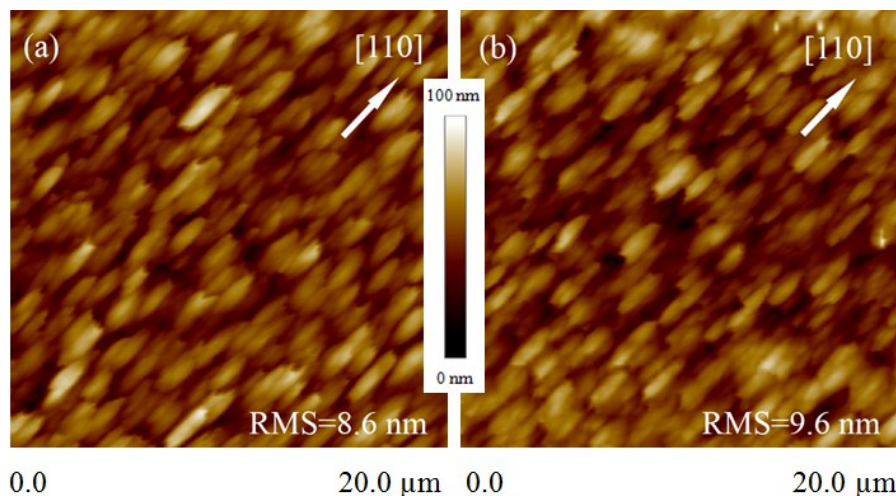
Fig. 3 20 × 20 μm² AFM images of the InAs/In$_{0.83}$Al$_{0.17}$As quantum well structures: grown on (a) Ga$_x$In$_{1-x}$P buffer (samples 1) and (b) GaAs$_y$P$_{1-y}$ buffer (samples 2)

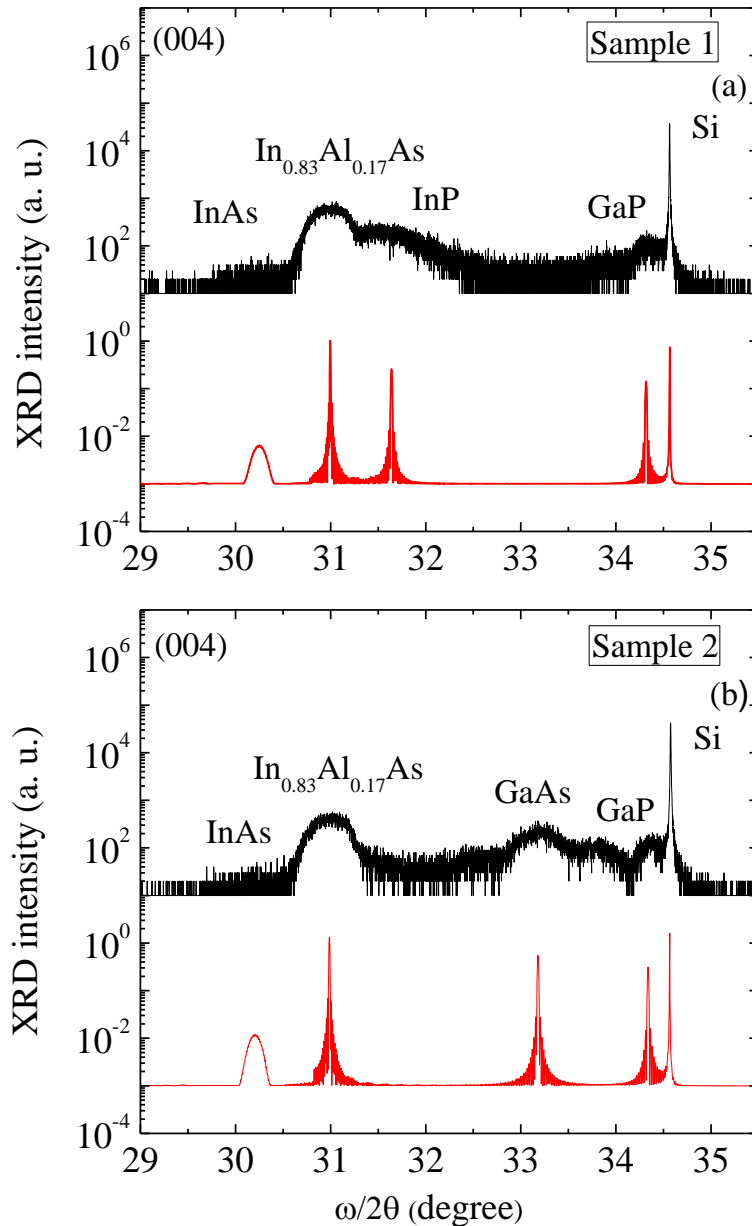图3 (a) Ga$_x$In$_{1-x}$P 缓冲层和(b) GaAs$_y$P$_{1-y}$ 缓冲层上生长的InAs/In$_{0.83}$Al$_{0.17}$As:量子阱结构的原子力显微镜照片,扫描范围为20×20 μm²

Fig. 4　HRXRD（004）scanning curves（the black one）and simulated curves（the red one）of the InAs/In$_{0.83}$Al$_{0.17}$As quantum well structures grown on（a）Ga$_x$In$_{1-x}$P buffer（sample 1）and（b）GaAs$_y$P$_{1-y}$ buffer（sample 2）
图4　（a）Ga$_x$In$_{1-x}$P 缓冲层和（b）GaAs$_y$P$_{1-y}$ 缓冲层上生长的 InAs/In$_{0.83}$Al$_{0.17}$As量子阱结构的（004）方向 HRXRD 扫描曲线（黑色线）和模拟曲线（红色线）

In the Fig. 5, the accurate strain relaxation state of the samples was investigated by the reciprocal space maps（RSMs）measurement involving the symmetric（004）as well as the asymmetric（115）reflections. In the RSMs figures, the relatively narrow and circular peaks are related to the Si substrate. The epitaxial layers with the elliptical shape corresponds to the In$_{0.83}$Al$_{0.17}$As virtual substrate. In the（004）RSMs of samples, between the Si substrate with the In$_{0.83}$Al$_{0.17}$As layer, the peaks corresponding to the GaP and InP layer have been denoted, respectively, in the sample with the Ga$_x$In$_{1-x}$P

buffer layer. As the Q$_y$ value is decreased, the three epitaxial layer peaks with broad distributions corresponds to the GaP buffer layer, the component gradient GaAs$_y$P$_{1-y}$ layer and the GaAs layer in the sample with the GaAs$_y$P$_{1-y}$, respectively. In the sample with the Ga$_x$In$_{1-x}$P layer, the position of the maximum diffraction intensity of the In$_{0.83}$Al$_{0.17}$As layer is close to the center of the Si substrate peak along the horizontal direction. However, in the other sample, the line connected with the center of the In$_{0.83}$Al$_{0.17}$As diffraction peak and the substrate peak shows slightly tilt with the vertical line. At the stressed

interfaces between III – V compound semiconductor materials, two types of misfit dislocations α and β, which is related to [-110] and [110] directions, respectively, may appear. The imbalanced glide velocities of the dislocations as well as the unequally activation energies for dislocation nucleation lead to the asymmetric strain relaxation, resulting in epilayer tilt in comparison to the substrate offcut axis. [30] The tilt resulted from different types of misfit dislocations is proportional to the substrate misorientation. Besides, the structure of the underlying buffer layer is verified to have a great effect on the crystallographic tilt [31]. Considering the same substrate offcut shared by the samples, the structures of the MBs which held an effect on the lattice relaxation process play a more important role on the tilt formation. Comparing to the step-graded sample, the relaxation process of a linearly-graded structures is slower since the strain energy in the later increases more gradually. Therefore, in the strain relaxation process of the $Ga_xIn_{1-x}P$ linear-graded sample, misfit dislocations have enough time to glide evenly towards [-110] and [110] directions, the lattice tilt is thus minimized in the InAlAs epilayers on the linear-graded buffer. [32] For the asymmetric (115) reflections, the lines of full relaxation and full pseudomorphic are drawn for references. The centers of the epitaxial layer contours are close to the relaxation line, indicating the strain of the sample has been relaxed through the compositionally graded Ga(In,As)P MBs and the $In_xAl_{1-x}As$ buf-

fer layers. In the symmetric (004) reflections, the broadening of the epitaxial layer contours along the Q_x caused by various mechanisms, such as mismatched dislocation, tilt formation, and anisotropy exiting in the layers. Among them, misfit dislocation plays a major role in the mechanisms. It can be extracted from the RSMs mapping, the broadening value of the $In_{0.83}Al_{0.17}As$ layer in sample 2 (44×10^4 rlu) is greater than that of sample 1 (36×10^4 rlu) along the Q_x, indicating the more misfit dislocations in the sample with the $GaAs_yP_{1-y}$ layer than the sample with the $Ga_xIn_{1-x}P$ MBs. Besides, the broadening along the Q_y reflects ingredient fluctuation of the component gradient buffer layer. Obviously, the broadening of the mosaic along the Q_x is greater than the broadening along the Q_y, indicating that the misfit dislocation is major factor deteriorating the material qualities while the component fluctuation plays a relatively minor factor.

The optical characteristics of the samples could be extracted from photoluminescence (PL) spectra. The PL spectra at different temperatures were measured by applying a Thermo Scientific Nicolet iS50 Fourier transform infrared (FTIR) spectrometer equipped with a liquid-nitrogen cooled InSb detector and CaF_2 beam splitter. A diode-pumped solid-state (DPSS) laser with the wavelength of 532 nm was used as the excitation source. The samples were mounted into a continuous-flow helium cryostat to change the temperature. The measurement temperature ranges from 10 K to RT. As shown in the
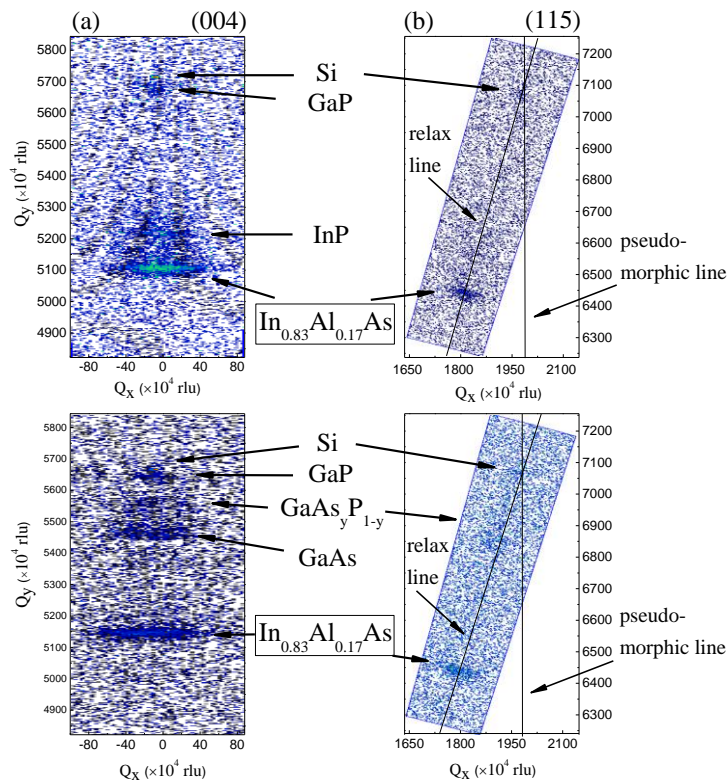

Fig. 5 Symmetric (004) and asymmetric (115) reciprocal space maps of the InAs/$In_{0.83}Al_{0.17}As$ quantum well structures grown on (a) $Ga_xIn_{1-x}P$ buffer and (b) $GaAs_yP_{1-y}$ buffer

图5 (a) $Ga_xIn_{1-x}P$ 缓冲层和(b) $GaAs_yP_{1-y}$ 缓冲层上生长的 InAs/$In_{0.83}Al_{0.17}As$ 量子阱结构 (004)对称和(115)非对称倒易空间衍射图

Fig. 6，the PL measurements were implemented under the selected temperature. In order to observe the data more clearly，the PL spectra have been enlarged for both samples under different temperature. The water absorption bands have been seen in the PL signals in the wavelength range of 2. 5-2. 8 μm. The PL emission peaks of both samples are around 2. 5 μm at 77 K and 2. 6 μm at RT，respectively.
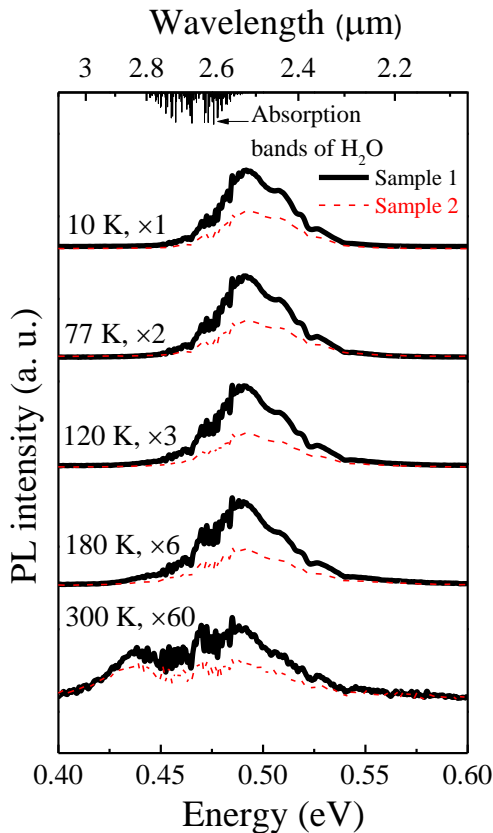

Fig. 6　PL spectra of sample 1（on $Ga_xIn_{1-x}P$ buffer）and sample 2（on $GaAs_yP_{1-y}$ buffer）
图 6　样品 1（$Ga_xIn_{1-x}P$ 缓冲层）和样品 2（$GaAs_yP_{1-y}$ 缓冲层）的光致发光图

The results extracted from the PL spectra have been reflected in the Fig. 7. Along with the temperature increasing，the PL intensities of the two samples are decreased. Meanwhile，the PL intensity of sample 1 with GaInP layer is about twice of sample 2 with GaAsP layer at selected temperature. The result indicates the lesser number of the non-radiative recombination centers in the InAs quantum well of the sample with GaInP layer. Simultaneously，the FWHMs of sample 2 are slightly larger than those of sample 1 at selected temperature，which reveals that there is lesser composition fluctuation and non-uniformity in the sample with GaInP. Besides，when the temperature increased，the fact that the scattering between phonons and excitons becomes stronger induces larger PL line width data of samples. It can be observed that the peak width of sample 2 is broadened much quick-

er than that of sample 1 when the temperature increased from 160 K to 300 K. It indicates that the scattering between phonons and excitons in the sample with GaAsP is stronger than those of the sample with GaInP in that temperature interval. The larger strain may exist in the well layers of sample 2，so the strain is easier to relax in the interface between InAs quantum well and $In_{0.83}Al_{0.17}As$ barrier layer. The breakdown of bonding at the interface may provide the more localization of longitudinal optical phonon. Thus，the strength of scattering between phonons and excitons is bigger in the sample with GaAsP than the other sample. [33]

The high indium fraction GaInP layer grown by GSMBE systems have been found to show unusual details at the growth surface [34]. The phase separation misoriented off ｛110｝ planes is generated in the area with the indium clustering，the features of the planar defects were termed “branch defects”. Branch defects have been shown to pin threading dislocations，causing the dislocation density escalation [35]. McGill et al. have confirmed high growth temperature delayed the branch defects formation in the high indium fraction GaInP graded buffer layer. [36] Besides，the local phase separation could be suppressed by the high V/III ratio effectively [37]. In the experiment，the relatively high growth temperature as well as the sufficient V/III ratio has been adopted to reduce the branch defects formation in the GaInP layer.

Depend on the broadening value of the $In_{0.83}Al_{0.17}As$ layer in RSMs measurement as well as the PL intensity of the InAs QW，the sample with compositional graded $Ga_xIn_{1-x}P$ buffer layer has slightly better properties than the sample with the step-graded $GaAs_yP_{1-y}$ layer. The growth temperature changed slowly during the growth of the $Ga_xIn_{1-x}P$ compositional graded buffer layer. Thus，the accurate Ga_2：In_2 flux ratio could be obtained to control the composition of the $Ga_xIn_{1-x}P$ MBs. The ternary layer could relax the strain between the GaP layer and $In_{0.83}Al_{0.17}As$ layer prominently. In addition，the propagation of threading dislocations originated from the GaP homoepitaxy and the GaP/Si substrate might be restrained effectively in the $Ga_xIn_{1-x}P$ buffer layer. Differently，during the growth of the $GaAs_yP_{1-y}$ step graded buffer layer，the AsH_3 and PH_3 are pumped into the Al_2O_3 ceramic tube and decomposed into hydrogen，As_4 and P_4 in the gas-cracking cells. Then，the As_4 and P_4 are cracking into As_2 and P_2 in the tiny pores at the bottom of the ceramic tube. The flux of the group V is controlled by the pressure differential between the biopolymer molecule and the vacuum chamber. Because the pressure in the growth chamber has a fluctuation，so，the flux of the group V is uneasy to control. The $GaAs_yP_{1-y}$ buffer layer with the imprecise quantities of atoms As and P might not relax the strain between the GaP layer and $In_{0.83}Al_{0.17}As$ layer sufficiently.

3　Conclusions

The InAs/$In_{0.83}Al_{0.17}As$ QWs with different buffer grading schemes from GaP to $In_{0.83}Al_{0.17}As$ virtual substrate are investigated. The graded buffers with mixed anions（GaAsP）and mixed cations（GaInP）were applied

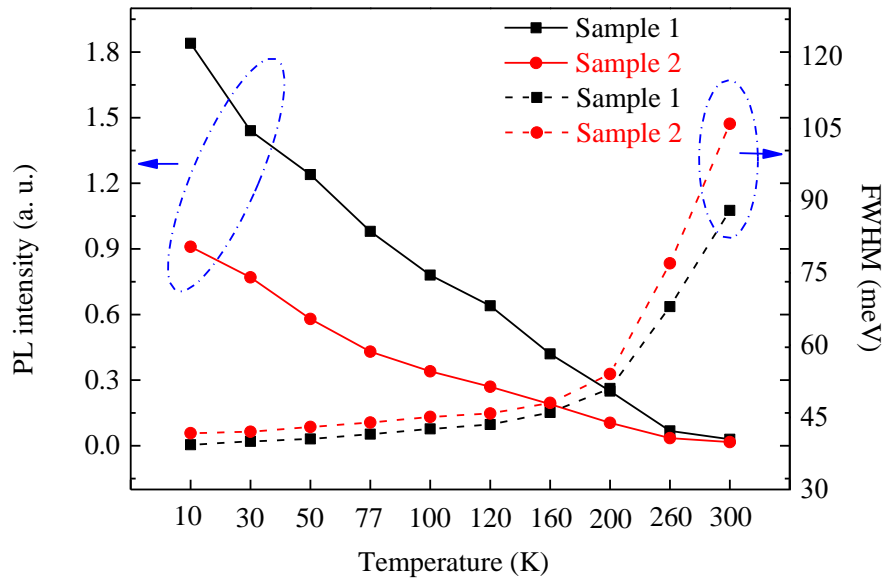Fig. 7 Temperature-dependent PL intensity and FWHM of sample 1 (on $Ga_xIn_{1-x}P$ buffer) and sample 2 (on $GaAs_yP_{1-y}$ buffer)

图7 样品1(包含$Ga_xIn_{1-x}P$缓冲层)和样品2(包含$GaAs_yP_{1-y}$缓冲层)的变温光致发光峰强度和半峰宽

and compared. The samples show similar surface morphology, close HRXRD FWHMs as well as close relaxation degree. The sample with $GaAs_yP_{1-y}$ buffer layer shows larger broadening of the epitaxial layer contours along the Q_x direction in HRXRD RSM, indicating more misfit dislocations than that on the $Ga_xIn_{1-x}P$ buffer. The PL emission peaks up to around 2.6 μm were observed for both samples at RT. The PL intensity of the sample on GaInP buffer is stronger than that on GaAsP buffer at various temperatures. These results give a potential pathway to improve the performance of mid-infrared light sources on GaP/Si substrate using mixed cation buffer layers.

Acknowledgment

References

[1] Wang H L, Wang F, Xia H, et al. Direct observation and manipulation of hot electrons at room temperature [J]. National Science Review, 2020, https://doi.org/10.1093/nsr/nwaa295.

[2] Ran W H, Wang L L, Zhao S F, et al. An integrated flexible all-nanowire infrared sensing system with record photosensitivity [J]. Advanced Materials, 2020, 32(16): 1908419.

[3] Sun M, Yu B C, Hong M Y, et al. Controlling the Facet of ZnO during Wet Chemical Etching Its (0001) O-Terminated Surface [J]. Small, 2020, 16(51): 2007045.

[4] Kumari B, Varshney R K, Pal B P. Design of chip scale silicon rib slot waveguide for sub-ppm detection of N_2O gas at mid-IR band [J]. Sensor. Actuat. B. Chem, 2018, 255: 3409-3416.

[5] Delli E, Letka V, Hodgson P D, et al. Mid-Infrared InAs/InAsSb Superlattice nBn Photodetector Monolithically Integrated onto Silicon [J]. Acs. Photonics, 2019, 6(2): 538-544.

[6] Jahromi K E, Pan Q, Hogstedt L, et al. Mid-infrared supercontinuum-based upconversion detection for trace gas sensing [J]. Opt. Express, 2019, 27(17): 24469-24480.

[7] Sergent S, Moreno J C, Frayssinet E, et al. GaN Quantum Dots Grown on Silicon for Free-Standing Membrane Photonic Structures [J]. Appl. Phys. Express, 2009, 2(5): 051003.

[8] Benyoucef M, Usman M, Reithmaier J P. Bright light emissions with narrow spectral linewidths from single InAs/GaAs quantum dots directly grown on silicon substrates [J]. Appl. Phys. Lett, 2013, 102 (13): 132101.

[9] Halioua Y, Bazin A, Monnier P, et al. Hybrid III-V semiconductor/silicon nanolaser [J]. Opt. Express, 2011, 19(10): 9221-9231.

[10] Tournie E, Cerutti L, Rodriguez J B, et al. Metamorphic III-V semiconductor lasers grown on silicon [J]. Mrs. Bull, 2016, 41(3): 218-223.

[11] Jung S, Kirch J, Kim J H, et al. Quantum cascade lasers transfer-printed on silicon-on-sapphire [J]. Appl. Phys. Lett, 2017, 111 (21): 211102.

[12] Nguyen-Van H, Baranov A N, Loghmari Z, et al. Quantum cascade lasers grown on silicon [J]. Sci. Rep, 2018, 8: 7206.

[13] Jung D, Yu L, Wasserman D, et al. Mid-infrared electroluminescence from InAs type-I quantum wells grown on InAsP/InP metamorphic buffers [J]. J. Appl. Phys, 2015, 118(18): 183101.

[14] Jung D, Yu L, Dev S, et al. Design and growth of multi-functional InAsP metamorphic buffers for mid-infrared quantum well lasers on InP [J]. J. Appl. Phys, 2019, 125(8): 082537.

[15] Tanabe K, Watanabe K, Arakawa Y. III-V/Si hybrid photonic devices by direct fusion bonding [J]. Sci. Rep, 2012, 2: 349.

[16] Qiang L, May L K. Epitaxial growth of highly mismatched III-V materials on (001) silicon for electronics and optoelectronics [J]. Prog. Cryst. Growth Charact. Mater, 2017, 63(4): 105-120.

[17] Liu H. Silicon-Based III-V Quantum Dot Materials and Dsevices: 2018 Conference on Lasers and Electro-Optics Pacific Rim, 2018 [C]. Hong Kong: IEEE, 2018: 18635366.

[18] Hu Y, Liang D, Mukherjee K, et al. III/V-on-Si MQW lasers by using a novel photonic integration method of regrowth on a bonding template [J]. Light. Sci. Appl, 2019, 8(5): 93.

[19] Li W, Anantha P, Bao S Y, et al. Germanium-on-silicon nitride waveguides for mid-infrared integrated photonics [J]. Appl. Phys. Lett, 2016, 109(24): 241101.

[20] Yamane K, Kawai T, Furukawa Y, et al. Growth of low defect density GaP layers on Si substrates within the critical thickness by opti-

mized shutter sequence and post-growth annealing ［J］. *J. Cryst. Growth*，2010，**312**（15）：2179-2184.

［21］Doescher H，Borkenhagen B，Lilienkamp G，*et al*. III-V on silicon：Observation of gallium phosphide anti-phase disorder by low-energy electron microscopy ［J］. *Surf. Sci*，2011，**605**（15-16）：L38-L41.

［22］Kemper R M，Schupp T，Haeberlen M，*et al*. Anti-phase domains in cubic GaN ［J］. *J. Appl. Phys*，2011，**110**（12）：123512.

［23］Volz K，Beyer A，Witte W，*et al*. GaP-nucleation on exact Si（001）substrates for III/V device integration ［J］. *J. Cryst. Growth*，2011，**315**（1）：37-47.

［24］Song Y F，Kujofsa T，Ayers J E. Threading Dislocations in InGaAs/GaAs（001）Buffer Layers for Metamorphic High Electron Mobility Transistors ［J］. *J. Electron. Mater*，2018，**47**（7）：3474-3482.

［25］Kujofsa T，Ayers J E. Lattice relaxation and misfit dislocations in nonlinearly graded $In_xGa_{1-x}As/GaAs$（001）and $GaAs_{1-y}P_y/GaAs$（001）metamorphic buffer layers ［J］. *J. Vac. Sci. Technol. B*，2014，**32**（3）：031205.

［26］Li K L，Sun Y R，Dong J R，*et al*. Control of threading dislocations by strain engineering in GaInP buffers grown on GaAs substrates ［J］. *Thin Solid Films*，2015，**593**：193-197.

［27］Wu J，Jiang Q，Chen S M，*et al*. Monolithically Integrated InAs/GaAs Quantum Dot Mid-Infrared Photodetectors on Silicon Substrates ［J］. *Acs Photonics*，2016，**3**（5）：749-753.

［28］Huang W G，Gu Y，Chen X Y，*et al*. Mid-infrared type-I InAs/$In_{0.83}Al_{0.17}$As quantum wells grown on GaP by gas source molecular beam epitaxy ［J］. *J. Cryst. Growth*，2019，**512**：61-64.

［29］Roesener T，Döscher H，Beyer A，*et al*. MOVPE growth of III-V solar cells on silicon in 300 mm closed coupled showerhead reactor：

25th European Photovoltaic Solar Energy Conf. and Exhibition，2010 ［C］. Valencia：**2010**：964–968.

［30］Goldman R S，Wieder H H，Kavanagh K L. Correlation of anisotropic strain relaxation with substrate misorientation direction at InGaAs/GaAs（001）interfaces ［J］. *Appl. Phys. Lett*，1995，**67**（3）：344.

［31］Ayers J E，Ghandhi S K，Schowalter L J. Crystallographic tilting of heteroepitaxial layers ［J］. J. *Cryst. Growth*，1991，**113**（3-4）：430-440.

［32］Chyi J-I，Shieh J-L，Pan J-W，*et al*. Material properties of compositional graded $In_xGa_{1-x}As$ and $In_xAl_{1-x}As$ epilayers grown on GaAs substrates ［J］. *J. Appl. Phys*，1996，**79**（11）：8367.

［33］Lei H P，Wu H Z，Lao Y F，*et al*. Difference of luminescent properties between strained InAsP/InP and strain-compensated InAsP/InGaAsP MQWs ［J］. *J. Cryst. Growth*，2003，**256**（1-2）：96-102.

［34］Park K W，Park C Y，Ravindran S，*et al*. Effect of post-annealing process on the optical properties of lateral composition-modulated GaInP structure grown by molecular beam epitaxy ［J］. *J. Mater. Sci*，2014，**49**（3）：1034-1040.

［35］Quitoriano N J，Fitzgerald E A. Relaxed，high-quality InP on GaAs by using InGaAs and InGaP graded buffers to avoid phase separation ［J］. *J. Appl. Phys*，2007，**102**（3）：033511.

［36］McGill L M，Fitzgerald E A，Huang J W，*et al*. Microstructural defects in metalorganic vapor phase epitaxy of relaxed，graded InGaP：Branch defect origins and engineering ［J］. *Sci. Technol*，2004，**22**（4）：1899.

［37］Stringfellow G B. Materials issues in high-brightness light-emitting diodes ［J］. *Semiconductors and Semimetals*，1997，**48**：1–45.